Supplementary Information for

Moving Beyond the Constraints of Chemistry *via* Crystal Structure Discovery with Isotropic Multiwell Pair Potentials

Julia Dshemuchadse, Pablo F. Damasceno, Carolyn L. Phillips, Michael Engel, and Sharon C. Glotzer

Corresponding author: Sharon C. Glotzer
E-mail: sglotzer@umich.edu

This PDF file includes:

Molecular Dynamics Simulations

The Molecular Dynamics (MD) simulations presented in this study were performed with the HOOMD-blue software package ([1–4]), simulating point particles that interact *via* Lennard-Jones Gauss potentials (LJGPs) and oscillating pair potentials (OPPs).

While both OPP and LJGP models are relatively short-ranged and exhibit steep repulsive forces at small r, they differ slightly in the types of functional shapes that they can adopt: the minima positions in OPP are strictly correlated (and determined *via* the k parameter) while the two minima in LJGP have different relative positions (defined by parameter r_0). The number of attractive minima in the OPP is always two, while a third minimum at low r-values can appear in addition. Depending on the separation of the LJ and Gaussian wells, the LJGP can exhibit one or two attractive minima. Furthermore, the OPP exhibits repulsive maxima between all minima, while the maximum between the LJGP minima is always in the attractive range.

In the LJGP system, a total of 5500 different state points were simulated. A first sweep of the entire phase diagram was performed with systems of $N = 2744$ particles per simulation that were cooled on a linear temperature ramp from $T = 3.0$ to 0.1 over 15×10^6 MD steps. In a second set of simulations – of 1379 of these state points – we performed longer simulations that corresponded effectively to a slower cooling of these same systems over 75×10^6 MD steps. A third set of simulations – of 138 state points – was performed in a region where no order had been observed to this point; here we divided the total simulation into two separate cooling ramps of temperatures from $T = 3.0$ *via* $T = 0.5$ down to $T = 0.1$ over $(11 + 275) \times 10^6$ MD steps. Additional simulations with different temperature profiles (some starting at lower temperatures, others introducing heating ramps followed by cooling) over a variety of MD steps and partially for larger systems were performed in regions of the phase diagram where no order had been observed thus far. These runs covered a total of 82 state points and were conducted over several more complex heating cycles to accommodate for the varying melting temperatures throughout the phase diagram.

In the OPP system, a total of 3052 different state points were simulated. A first sweep of the entire phase diagram was performed with systems of $N = 4096$ particles per simulation that were cooled on a linear temperature ramp from $T = 0.6$ to 0.01 over 60×10^6 MD steps.

Known Structure Types

16 structures found in this study were found to have equivalent structures on the atomic scale. Details on these structures are listed in Tab. S1.

New Structure Types – Ordered Structures

15 structures found in this study were not found to have any known equivalents on the atomic scale. Here, this is denoted by an X in place of the chemical formula in the Pearson symbol. The simplest of these new structures is $hP1$-X—illustrated in Fig. S1, which consists of stacked layers corresponding to triangular lattices. The $hP2$-X structure has the same Pearson symbol and space group (as well as the Wyckoff position) as the $hP2$-Mg structure type, however, due to a different c/a-ratio and consequently different coordination polyhedron (a bi-capped triangular prism instead of an anti-cuboctahedron), it can be regarded as a separate structure type.

The $oC20$-X and $oF64$-X structures are illustrated in Fig. S2. The $oC20$-X structure consists of slightly puckered square-lattice layers, as shown in Fig. S3.

The $hP10$-X, $hP18$-X, and $tI20$-X structures are illustrated in Fig. S4. The unit cell of the $hP10$-X structure type contains particles forming columns of face-sharing octahedra parallel to the c-direction, as well as twice as many intermediate columns of individual particles. The unit cell of the $hP18$-X structure type contains particles forming columns of face-sharing octahedra parallel to the c-direction at three different heights, describing all particles in the unit cell. The unit cell of the $tI20$-X structure type contains particles forming columns of face-sharing square antiprisms parallel to the c-direction, as well as the same number of intermediate columns of individual particles.

Different illustrations of the $hP14$-X structure are shown in Fig. S5. The unit cell of the $hP14$-X structure type also contains particles forming columns of face-sharing octahedra parallel to the c-direction, with an intermediate network of vertex- and face-sharing tetrahedra.

The $cI100$-X and $hR57$-X structures are illustrated in Fig. S6. All particles in the $hR57$-X structure type have coordination number 12, approximately a third of which corresponds to icosahedra (corresponding to two out of two Wyckoff positions), while the remaining ones are too distorted to be assigned a simple polyhedral shape.

The $oP52$-X structure is illustrated in Fig. S7. The $oP52$-X structure type has particles with coordination numbers between 8 and 12, forming a framework of square antiprisms, octahedra, tetrahedra, *etc.*, and exhibits strong tetragonal pseudo-symmetries.

The $oP28$-X structure is illustrated in Fig. S8. $oP28$-X is a Frank-Kasper phase, which had previously been postulated ([5]) (see Tab. 2, No. 7).

Julia Dshemuchadse, Pablo F. Damasceno, Carolyn L. Phillips, Michael Engel, and Sharon C. Glotzer

New Structure Types – Disordered Structures

The $tI8$-X structure type—illustrated in Fig. S9—is built from two alternating kinds of layers: a fully ordered, buckled square lattice and a disordered, flat triangle-square lattice. The latter can be present in two, equivalent orientations; since these layers are separated by the buckled square lattice, the occupancies of the disordered layer seem to be uncorrelated.

The unit cell of the $tI32$-X structure type—illustrated in Fig. S10—contains particles forming columns of edge-sharing tetrahedra parallel to the c-direction, alternating with columns of individual particles. Since the latter are separated entirely by particles in the columns of tetrahedra, their exact heights are not connected and columns of particles at three equivalent heights occur in an uncorrelated manner.

The $tI2.2$-X structure type—also illustrated in Fig. S10—is mostly built from widely-spaced square layers, with an interstitial site that is occupied at 5%, forming square pyramids.

Bond-Orientational Order Diagrams

Bond-orientational order diagrams (BODs) for the observed structures are shown in Fig. S11 for the previously known structures, and in Fig. S12 for the new ones.

Radial distribution functions *vs.* interaction potentials

Examples for interaction potentials and the radial distribution functions of the assembled particle arrangements are given for all observed structure types: in Fig. S13 for structures with coordination numbers $CN = 3.4 - 5.0$, in Fig, S14 for structures with coordination number $CN = 6$, in Fig. S15 for structures with coordination numbers $CN = 7.0 - 8$, in Fig. S16 for structures with coordination numbers $CN = 8.8 - 9.3$, in Fig. S17 for structures with coordination numbers $CN = 10.0 - 11.3$, in Fig. S18 for structures with coordination number $CN = 12$, in Fig. S19 for structures with coordination numbers $CN = 12.6 - 13.5$, and in Fig. S20 for structures with coordination number $CN = 14$.

Phase diagram exploration

The pair potential parameter data used for the consecutive steps in the exploration of the phase diagrams are shown in Fig. S21 for OPP and in Fig. S22 for LJGP.

The locations of the different crystal phases in the OPP and LJGP phase diagrams are indicated in Figs. S23 and S24.

Table S1. Representative structure data of previously known crystal structures self-assembled from point particles interacting *via* the LJGP and OPP. FK14 and FK15 denote Frank-Kasper polyhedra with 14 and 15 vertices, respectively. Two-dimensional structures are marked with "*(2D)*". Distorted coordination polyhedra are denoted with "dist.".
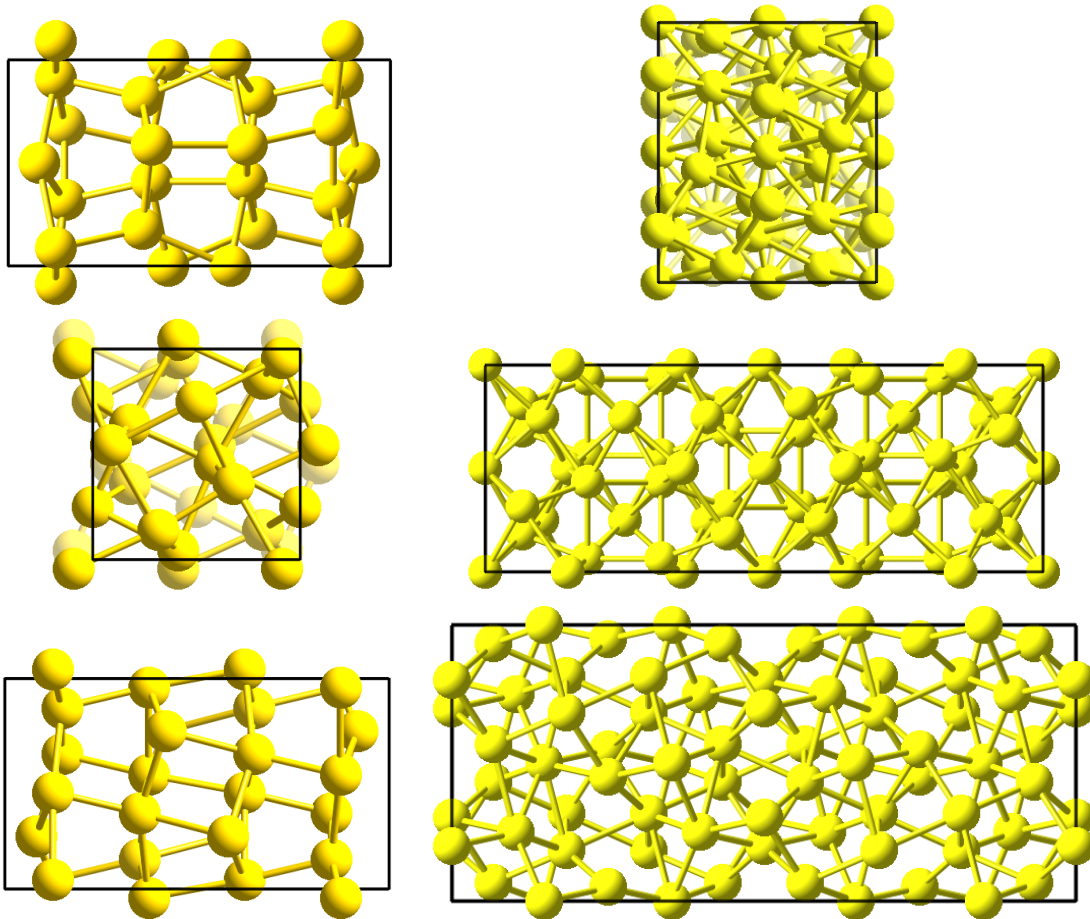
Structure type	Space group	Wyckoff sites	Coordination numbers & polyhedra
$cP54$-K_4Si_{23}	$Pm\bar{3}n$	$2a\ 0,0,0$	CN0 = $\varnothing$
		$6d\ 1/4, 1/2, 0$	CN0 = $\varnothing$
		$6c\ 1/4, 0, 1/2$	CN4 = tetrahedron
		$16i\ x,x,x\ (x = 0.315)$	CN4 = tetrahedron
		$24k\ 0,y,z\ (y = 0.307, z = 0.120)$	CN4 = tetrahedron
$cI16$-Si	$Ia\bar{3}$	$16c\ x,x,x\ (x = 0.854)$	CN4 = tetrahedron
$tI2$-CdHg	$I4/mmm$	$2a\ 0,0,0$	CN4 = square *(2D)*
	$(c/a = 2.17)$		
$cP1$-Po	$Pm\bar{3}m$	$1a\ 0,0,0$	CN6 = octahedron
$tI4$-Sn	$I4_1/amd$	$4a\ 0,0,0$ (origin choice 1)	CN6 = dist. octahedron
	$(c/a = 0.58)$		
$cP4$-Li	$P4_332$	$8c\ x,x,x\ (x = 0.625)$	CN6 = dist. triangular prism
$hP1$-$Ca_{0.15}Sn_{0.85}$	$P6/mmm$	$1a\ 0,0,0$	CN8 = hexagonal bipyramid
	$(c/a = 0.98)$		
$cF4$-Cu	$Fm\bar{3}m$	$4a\ 0,0,0$	CN12 = octahedron
$hP2$-Mg	$P6_3/mmc$	$2c\ 1/3, 2/3, 1/4$	CN12 = anti-cuboctahedron
	$(c/a = 1.54)$		
$cI52$-Cu_5Zn_8	$I\bar{4}3m$	$8c\ x,x,x\ (x = 0.401)$	CN12 = dist. icosahedron
		$8c\ x,x,x\ (x = 0.668)$	CN12 = dist. icosahedron
		$12e\ x,0,0\ (x = 0.353)$	CN13 = rhombic dodecahedron -1
		$24g\ x,x,z\ (x = 0.321, z = 0.984)$	CN13 = rhombic dodecahedron -1
$cP20$-Mn	$P4_332$	$8c\ x,x,x\ (x = 0.804)$	CN14 = dist. FK14 polyhedron
		$12d\ 1/8, y, -y+1/4\ (y = 0.693)$	CN12 = icosahedron
$hP7$-Zr_4Al_3	$P6/mmm$	$2d\ 1/3, 2/3, 1/2$	CN15 = FK15 polyhedron
	$(c/a = 1.05)$	$2e\ 0,0,z\ (z = 0.300)$	CN14 = FK14 polyhedron
		$3f\ 1/2, 0, 0$	CN12 = icosahedron
$tP30$-CrFe	$P4_2/mnm$	$2a\ 0,0,1/2$	CN12 = icosahedron
	$(c/a = 0.53)$	$4f\ x,x,0\ (x = 0.102)$	CN15 = FK15 polyhedron
		$8i\ x,y,0\ (x = 0.629, y = 0.964)$	CN14 = FK14 polyhedron
		$8i\ x,y,0\ (x = 0.433, y = 0.762)$	CN12 = icosahedron
		$8j\ x,x,z\ (x = 0.319, z = 0.750)$	CN14 = FK14 polyhedron
$cP8$-Cr_3Si	$Pm\bar{3}n$	$2a\ 0,0,0$	CN12 = icosahedron
		$6c\ 1/4, 0, 1/2$	CN14 = FK14 polyhedron
$cI2$-W	$Im\bar{3}m$	$2a\ 0,0,0$	CN14 = rhombic dodecahedron
$tI2$-Pa	$I4/mmm$	$2a\ 0,0,0$	CN14 = dist. rhomb. dodecahedron
	$(c/a = 0.81)$		

Julia Dshemuchadse, Pablo F. Damasceno, Carolyn L. Phillips, Michael Engel, and Sharon C. Glotzer

Table S2. Representative structure data of novel crystal structures self-assembled from point particles interacting *via* the LJGP and OPP. Two-dimensional structures are marked with "*(2D)*". Distorted coordination polyhedra are denoted with "dist.". Coordination polyhedra with ambiguous shapes are denoted with "?".

| Structure type	Space group	Wyckoff sites	Coordination numbers & polyhedra
$hP1$-X	$P6/mmm$	$1a$ $0, 0, 0$	CN6 = hexagon *(2D)*
	($c/a = 1.48$)		
$oC20$-X	$C222_1$	$4b$ $0, y, 1/4$ ($y = 0.419$)	CN6 = dist. triangular prism
	($c/a = 1.01$)	$8c$ x, y, z ($x = 0.912, y = 0.125, z = 0.958$)	CN6 = octahedron
	($b/a = 1.85$)	$8c$ x, y, z ($x = 0.319, y = 0.851, z = 0.860$)	CN6 = dist. octahedron
$oF64$-X	$Fddd$	$16f$ $0, y, 0$ ($y = 0.801$) (origin choice 1)	CN6 = dist. octahedron
	($c/a = 2.71$)	$16g$ $0, 0, z$ ($z = 0.148$)	CN8 = ?
	($b/a = 1.19$)	$32h$ x, y, z ($x = 0.065, y = 0.683, z = 0.184$)	CN7 = ?
$hP2$-X	$P6_3/mmc$	$2c$ $1/3, 2/3, 1/4$	CN8 = bi-capped triangular prism
	($c/a = 0.64$)		
$hP10$-X	$P6_3/mcm$	$4d$ $1/3, 2/3, 0$	CN8 = dist. cube
	($c/a = 0.77$)	$6g$ $x, 0, 1/4$ ($x = 0.750$)	CN10 = pentagonal prism
$tI20$-X	$I4/mcm$	$4b$ $0, 1/2, 1/4$	CN10 = ?
	($c/a = 0.55$)	$16k$ $x, y, 0$ ($x = 0.713, y = 0.573$)	CN9 = ?
$cI100$-X	$Im\bar{3}m$	$12e$ $x, 0, 0$ ($x = 0.843$)	CN12 = dist. cuboctahedron
		$16f$ x, x, x ($x = 0.313$)	CN10 = ?
		$24h$ $0, y, y$ ($y = 0.379$)	CN8 = ?
		$48j$ $0, y, z$ ($y = 0.684, z = 0.840$)	CN9 = ?
$hP18$-X	$R\bar{3}c$	$18e$ $x, 0, 1/4$ ($x = 0.184$)	CN10 = ?
	($c/a = 0.53$)		
$oP52$-X	$Pbcm$	$4d$ $x, y, 1/4$ ($x = 0.244, y = 0.205$)	CN11 = cuboctahedron -1
	($c/a = 1.31$)	$4d$ $x, y, 1/4$ ($x = 0.552, y = 0.071$)	CN11 = dist. pentagonal prism $+1$
	($b/a = 1.00$)	$4d$ $x, y, 1/4$ ($x = 0.923, y = 0.436$)	CN12 = dist. pentagonal prism $+2$
		$8e$ x, y, z ($x = 0.544, y = 0.678, z = 0.610$)	CN10 = dist. pentagonal prism
		$8e$ x, y, z ($x = 0.174, y = 0.054, z = 0.880$)	CN10 = dist. pentagonal prism
		$8e$ x, y, z ($x = 0.665, y = 0.964, z = 0.921$)	CN11 = dist. pentagonal prism $+1$
		$8e$ x, y, z ($x = 0.958, y = 0.655, z = 0.414$)	CN10 = ?
		$8e$ x, y, z ($x = 0.754, y = 0.244, z = 0.377$)	CN9 = ?
$hP14$-X	$P6_3mc$	$2b$ $1/3, 2/3, z$ ($z = 0.505$)	CN12 = ?
	($c/a = 0.63$)	$6c$ $x, -x, z$ ($x = 0.126, z = 0.298$)	CN11 = ?
		$6c$ $x, -x, z$ ($x = 0.455, z = 0.000$)	CN11 = ?
$hR57$-X	$R\bar{3}$	$3a$ $0, 0, 0$ $1/3, 2/3, 2/3$	CN12 = icosahedron
	($c/a = 1.22$)	$18f$ x, y, z ($x = 0.153, y = 0.511, z = 0.475$)	CN12 = dist. icosahedron
		$18f$ x, y, z ($x = 0.414, y = 0.975, z = 0.697$)	CN12 = dist. icosahedron
		$18f$ x, y, z ($x = 0.147, y = 0.210, z = 0.414$)	CN12 = ?
$oP28$-X	$P2_12_12$	$2a$ $0, 0, z$ ($z = 0.940$)	CN12 = dist. icosahedron
	($c/a = 1.00$)	$2b$ $0, 1/2, z$ ($z = 0.202$)	CN12 = dist. icosahedron
	($b/a = 1.37$)	$4c$ x, y, z ($x = 0.687, y = 0.687, z = 0.296$)	CN12 = icosahedron
		$4c$ x, y, z ($x = 0.571, y = 0.132, z = 0.440$)	CN12 = icosahedron
		$4c$ x, y, z ($x = 0.811, y = 0.451, z = 0.852$)	CN12 = icosahedron
		$4c$ x, y, z ($x = 0.365, y = 0.771, z = 0.062$)	CN12 = dist. icosahedron
		$4c$ x, y, z ($x = 0.547, y = 0.666, z = 0.716$)	CN14 = FK14 polyhedron
		$4c$ x, y, z ($x = 0.316, y = 0.591, z = 0.419$)	CN14 = FK14 polyhedron
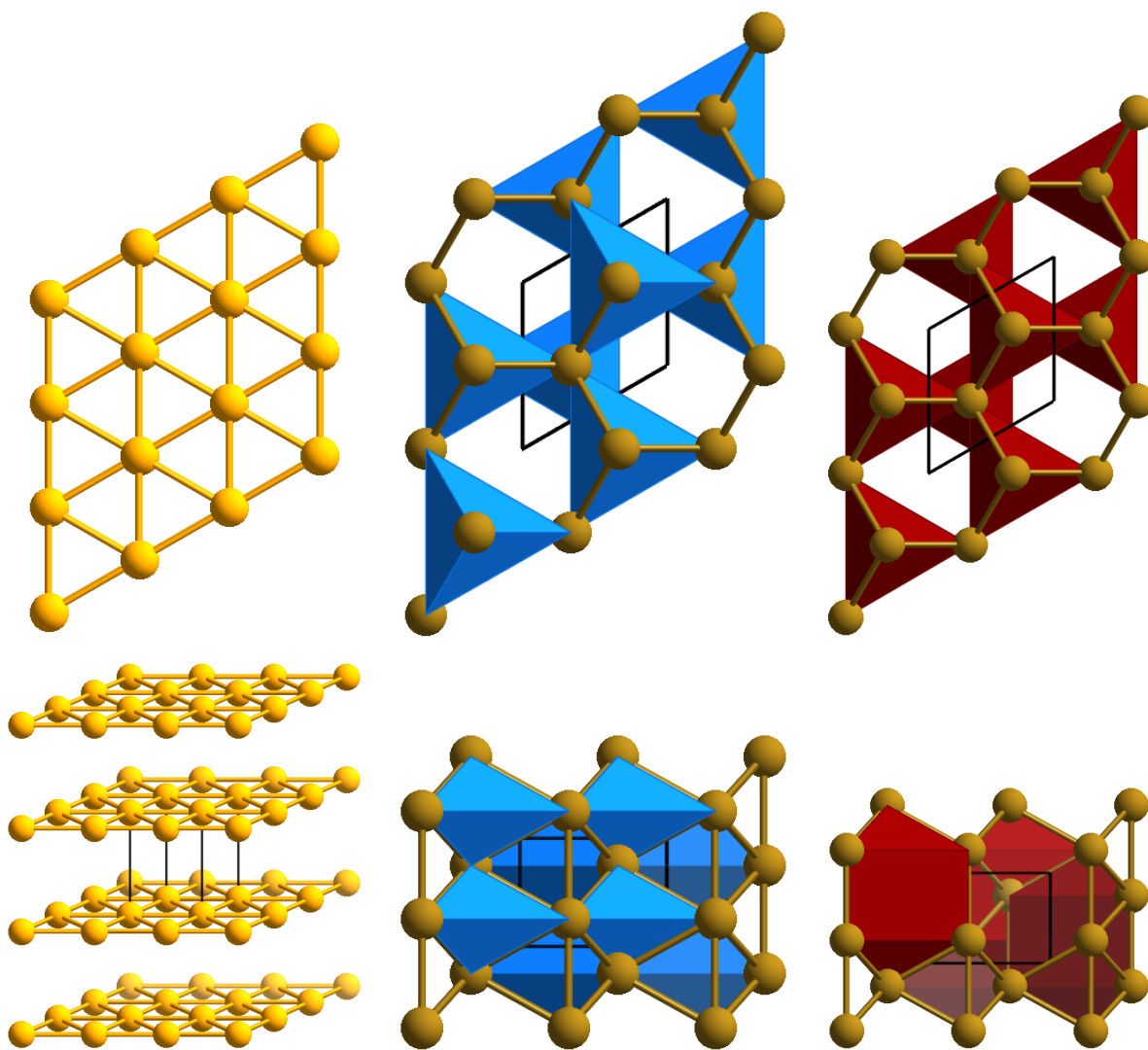
Fig. S1. $hP1\text{-}X$ (*left*) and $hP2\text{-}X$ structure (*middle and right*); projections along the $[001]$ direction (*top*), and at an angle (*bottom left*) as well as the $[100]$ direction (*bottom middle* and *bottom right*); inter-particle polyhedra – triangular bipyramids – are highlighted in blue (*middle*) and coordination polyhedra – bi-capped triangular prisms – are highlighted in red (*right*) in the $hP2\text{-}X$ structure; unit cells are represented by black outlines.

Julia Dshemuchadse, Pablo F. Damasceno, Carolyn L. Phillips, Michael Engel, and Sharon C. Glotzer

Fig. S2. $oC20$-X (*left*) and $oF64$-X structure (*right*); projections along the $[001]$, $[010]$, and $[100]$ directions (*top*), *middle*, and *bottom*, respectively); unit cells are represented by black outlines.
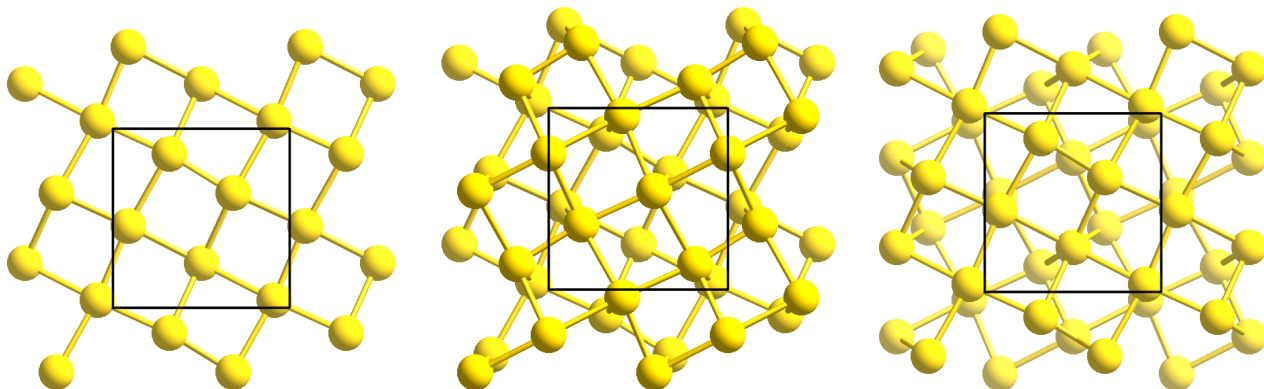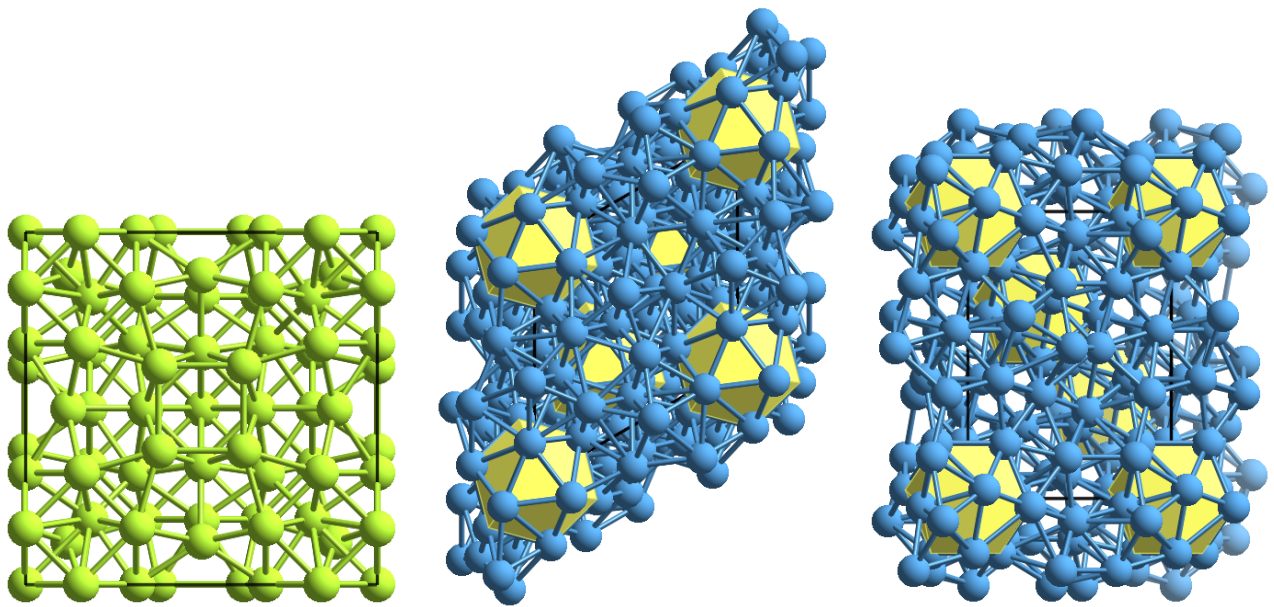
Fig. S3. Layers forming the $oC20\text{-}X$ structure, shown in projections along the $[010]$ direction; a single layer (*left*), as well as the combinations of the same layer with its immediate neighboring layers above and below (*middle* and *right*); the unit cell is represented by black outlines.
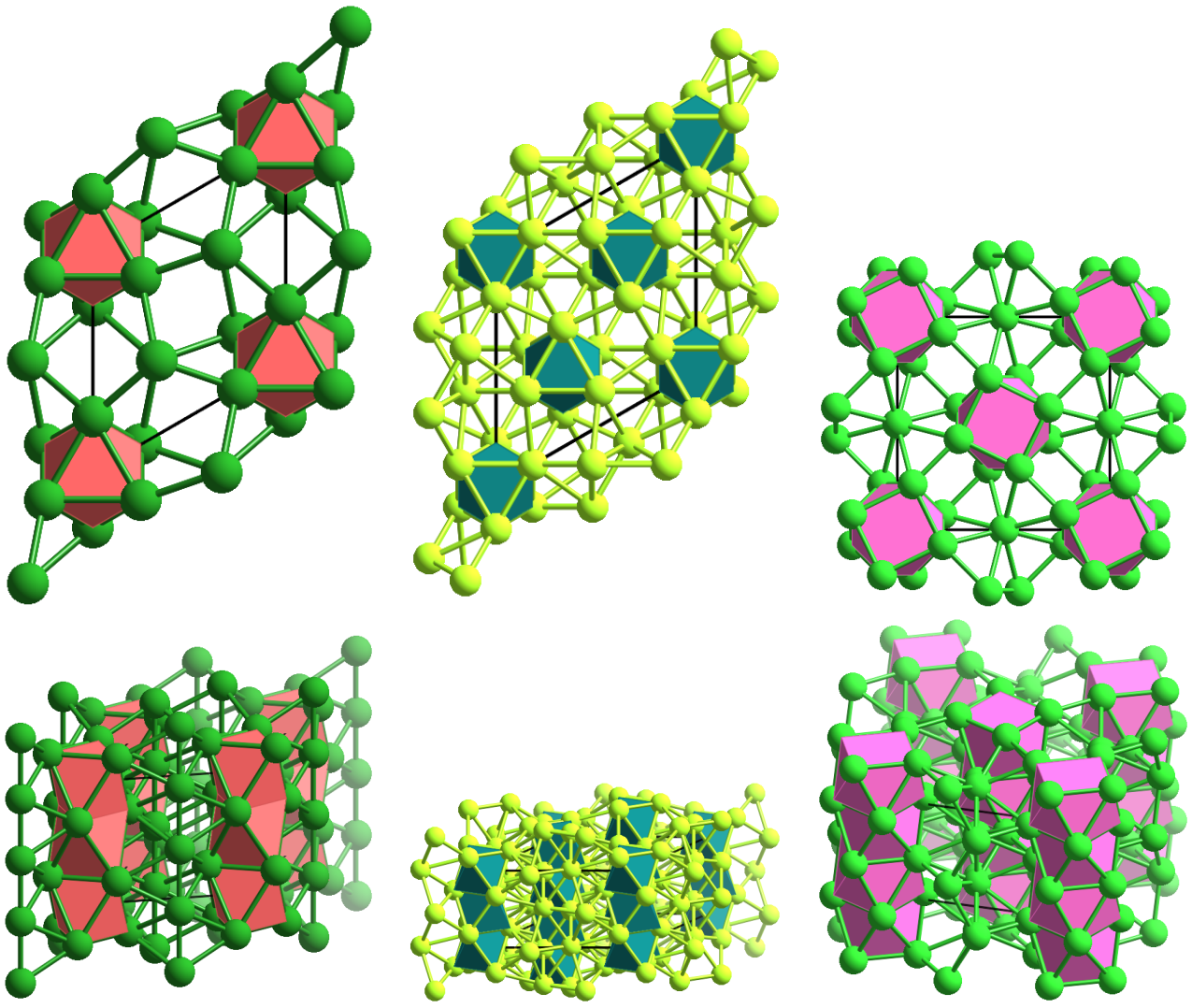
Fig. S4. $hP10\text{-}X$, $hP18\text{-}X$, and $tI20\text{-}X$ structures (*left* to *right*); projections along the $[001]$ direction (*top*) and at an angle (*bottom*); inter-particle polyhedra – octahedra, square antiprisms – are illustrated; unit cells are represented by black outlines.
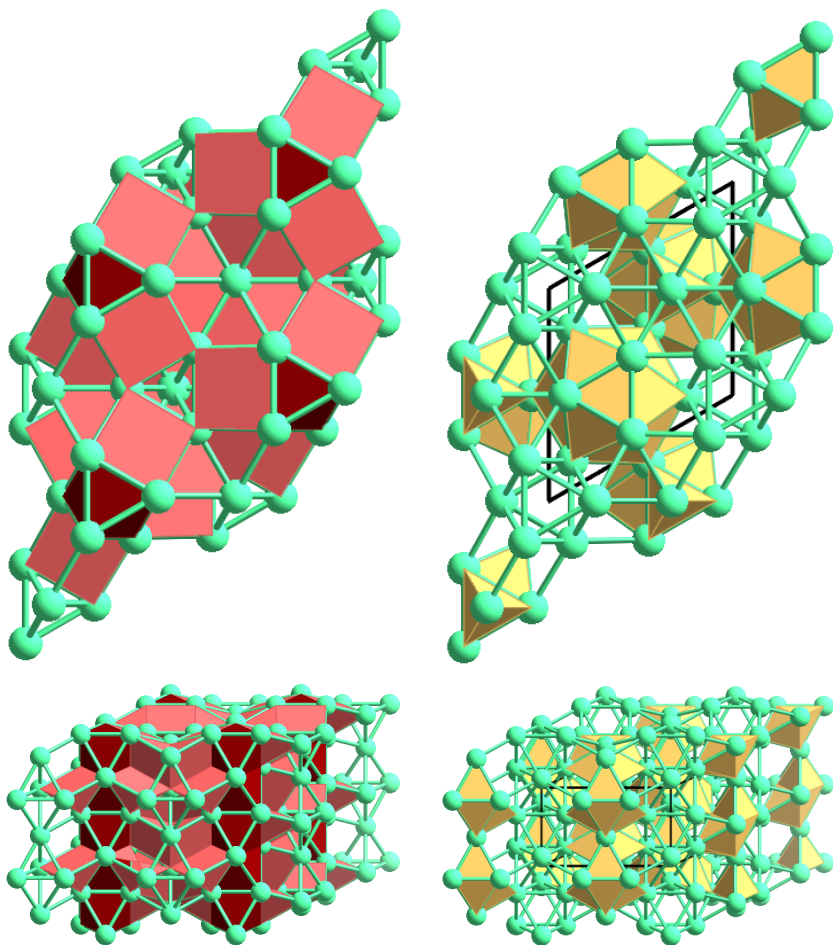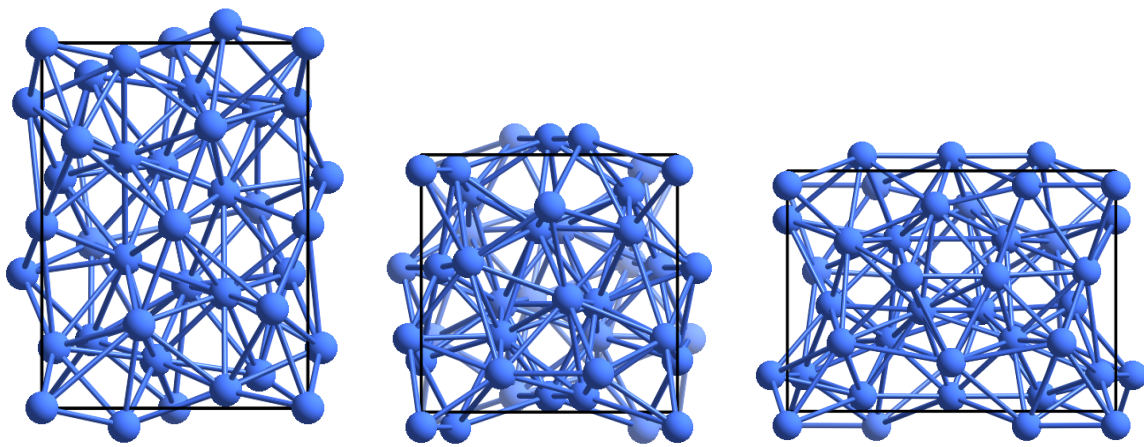
Fig. S5. $hP14$-X structure; projections along the $[001]$ direction (*top*) and at an angle (*bottom*); inter-particle polyhedra – octahedra and square pyramids in red and rose-colored, and tetrahedra in yellow – are illustrated; the unit cell is represented by black outlines.

Julia Dshemuchadse, Pablo F. Damasceno, Carolyn L. Phillips, Michael Engel, and Sharon C. Glotzer

Fig. S6. $cI100\text{-}X$ and $hR57\text{-}X$ structures; projection along the $[001]$ direction of the $cI100\text{-}X$ structure (*left*); projections along the $[001]$ and $[100]$ directions (*middle* and *right*, respectively) of the $hR57\text{-}X$ structure, in which icosahedral coordination polyhedra are illustrated; unit cells are represented by black outlines.
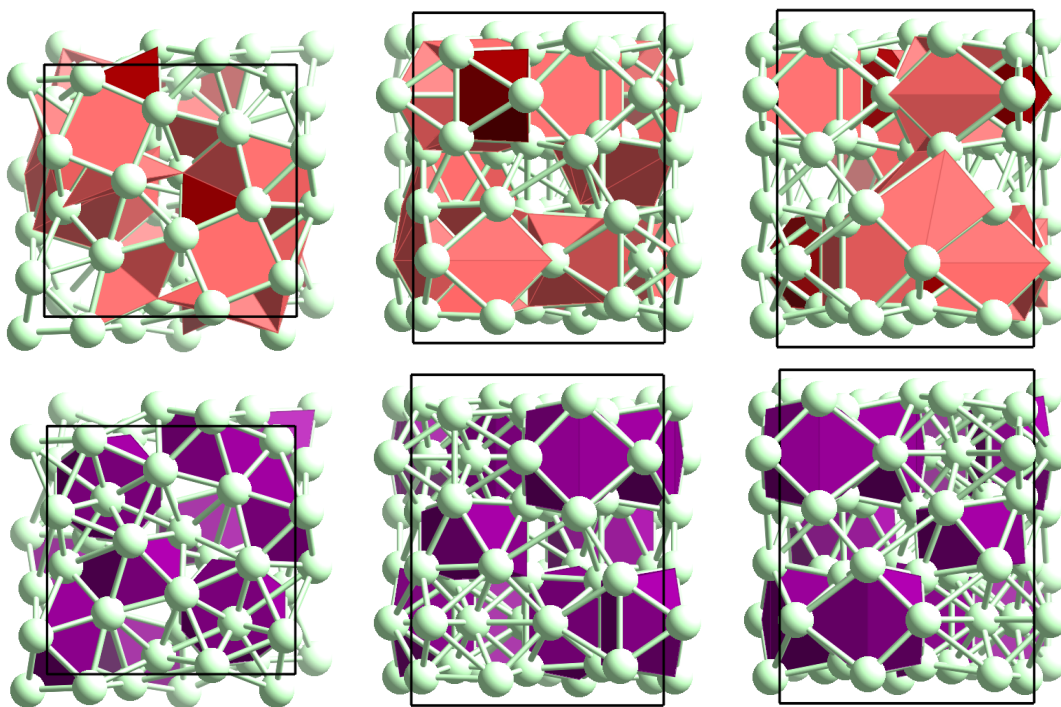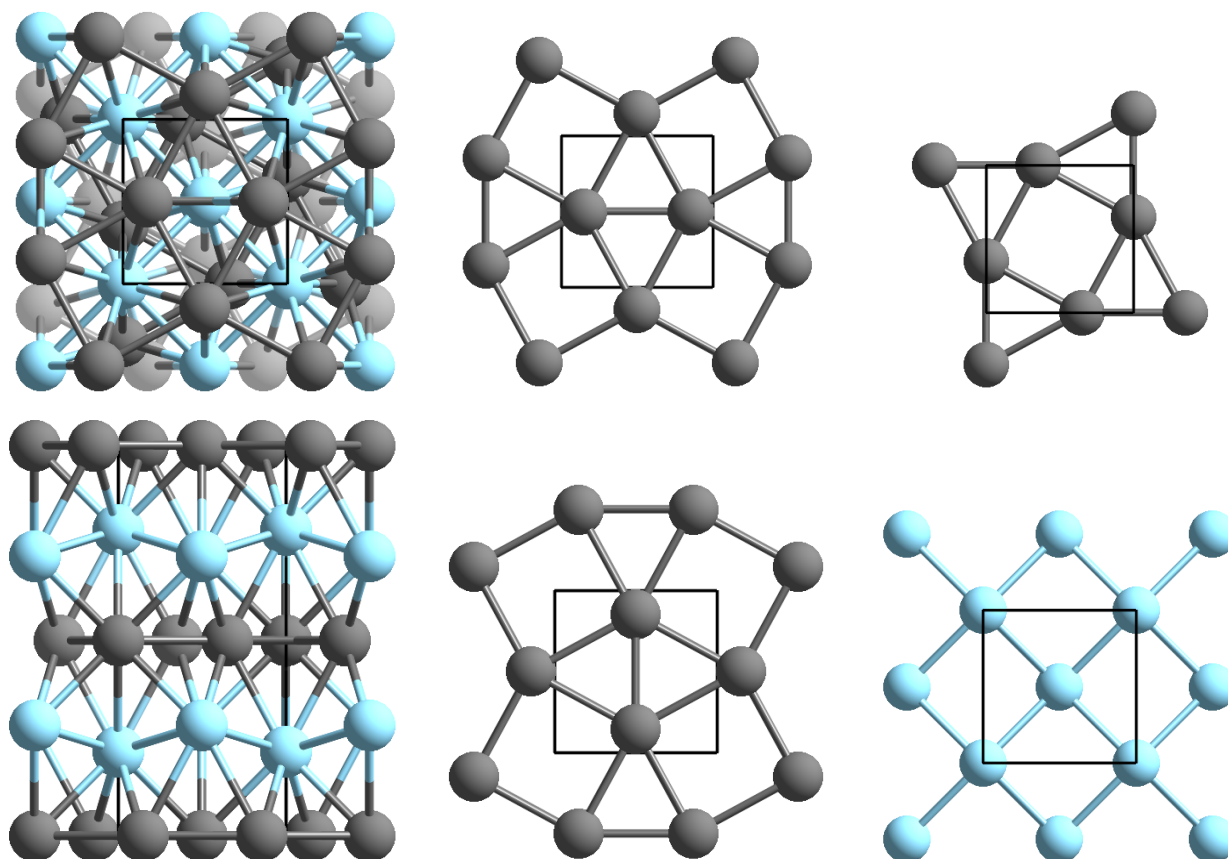
Fig. S7. $oP52$-X structure; projections along the $[001]$, $[010]$, and $[100]$ directions (*left* to *right*); inter-particle polyhedra – octahedra and square pyramids *top*, as well as square antiprisms *bottom* – are illustrated; the unit cell is represented by black outlines.

Julia Dshemuchadse, Pablo F. Damasceno, Carolyn L. Phillips, Michael Engel, and Sharon C. Glotzer

Fig. S8. $oP28\text{-}X$ structures; projections along the $[001]$, $[010]$, and $[100]$ directions (*left*) to *right*); the unit cell is represented by black outlines.

Table S3. Representative structure data of disordered novel crystal structures self-assembled from point particles interacting *via* the LJGP and OPP. Distorted coordination polyhedra are denoted with "dist.".

Structure type	Space group	Wyckoff sites	Coordination numbers & polyhedra
$tI2.2\text{-}X$	$I4/mmm$	$2a\ 0,0,0$	CN4–5 = square $(+1)$
	$(c/a = 3.08)$	$4e\ 0,0,z\ (z = 0.646)$ (occ. $= 0.05$)	CN5 = square pyramid
$tI32\text{-}X$	$I4/mcm$	$8h\ x, x + {}^{1}/2, 0\ (x = 0.149)$	CN9–CN11 = $\sim$
	$(c/a = 1.57)$	$16l\ x, x + {}^{1}/2, z\ (x = 0.350)$	CN9–CN11 = $\sim$
		$8f\ 0,0,z\ (z = 0.044)$ (occ. $= 0.333$)	CN8 = bi-capped triangular prism
		$8f\ 0,0,z\ (z = 0.124)$ (occ. $= 0.333$)	CN8 = bi-capped triangular prism
		$8f\ 0,0,z\ (z = 0.210)$ (occ. $= 0.333$)	CN8 = bi-capped triangular prism
$tI8\text{-}X$	$I4/mmm$	$4e\ 0,0,z\ (z = 0.783)$	CN12 = dist. cuboctahedron
	$(c/a = 2.33)$	$8j\ x, {}^{1}/2, 0\ (x = 0.852)$ (occ. $= 0.5$)	CN11 = capped pentagonal prism

Julia Dshemuchadse, Pablo F. Damasceno, Carolyn L. Phillips, Michael Engel, and Sharon C. Glotzer

Fig. S9. $tI8$-X structure; projections along the $[001]$ and $[100]$ directions (*top left* and *bottom left*, respectively); projections of separate layers along the $[001]$ direction: two alternative arrangements of a flat disordered layer (*top middle* and bottom middle), the shifted positions of a consecutive disordered layer (*top right*)), and a puckered ordered layer (*bottom right*); particles on the ordered site are shown in blue; particles on the disordered site – with 50% occupancy – are shown in dark gray color; unit cells are represented by black outlines.
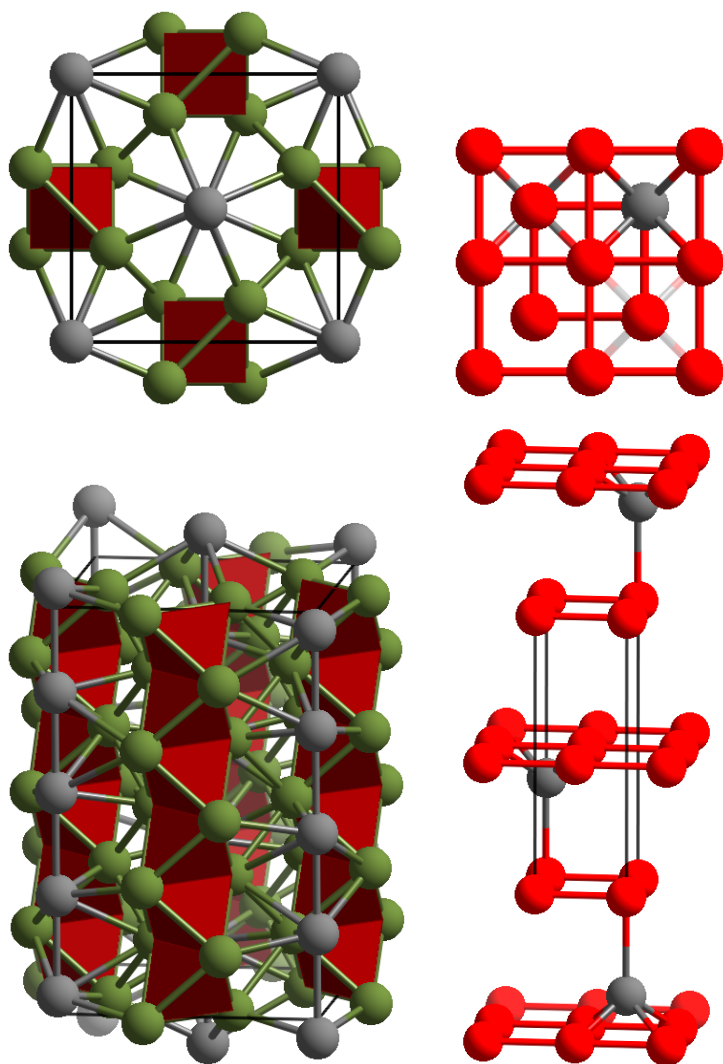
Fig. S10. $tI32\text{-}X$ and $tI2.2\text{-}X$ structures (*left* and *right*, respectively); projections along the $[001]$ direction (*top*) and at an angle (*bottom*); inter-particle polyhedra – tetrahedra – are highlighted in the $tI32\text{-}X$ structure; particles on the ordered sites are shown in green (*left*) and red (*right*); particles on the disordered sites – with 33% (*left*) and 5% occupancy (*right*), respectively – are shown in dark gray color; unit cells are represented by black outlines.
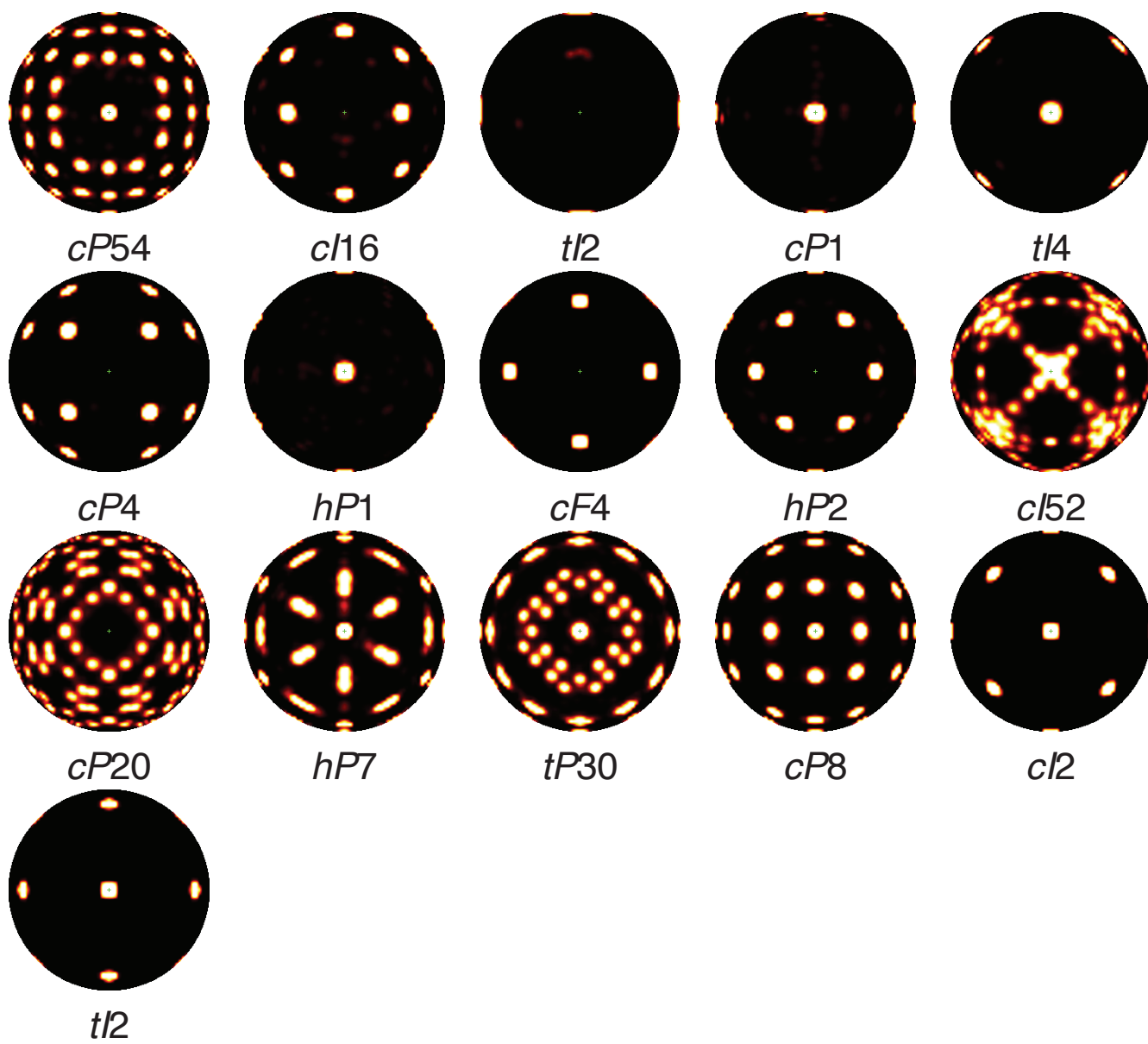
Julia Dshemuchadse, Pablo F. Damasceno, Carolyn L. Phillips, Michael Engel, and Sharon C. Glotzer

cP54   cI16   tI2   cP1   tI4

cP4   hP1   cF4   hP2   cI52

cP20   hP7   tP30   cP8   cI2

tI2

Fig. S11. Bond-orientational order diagrams (BODs) of the observed structures with previously known atomic equivalents.
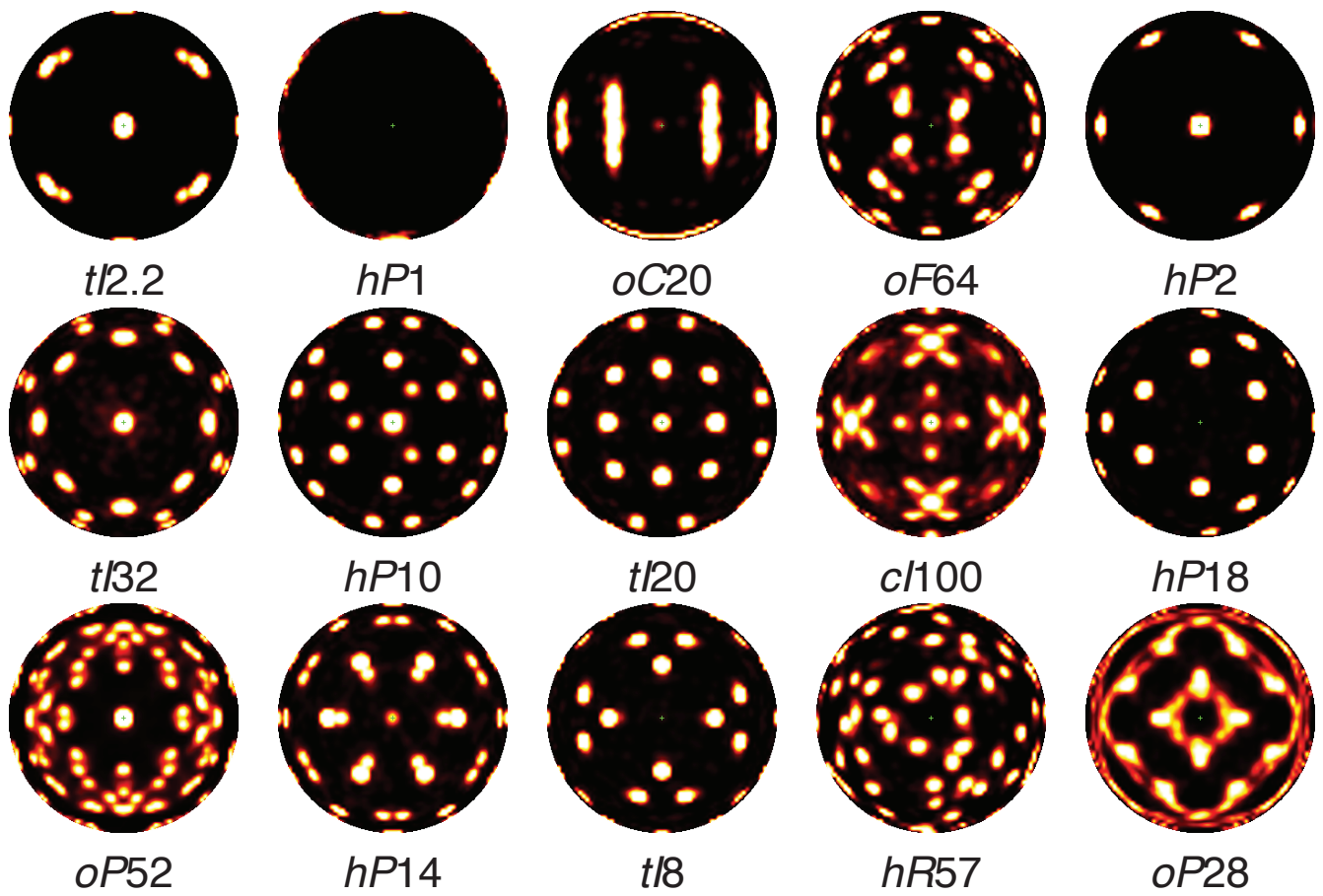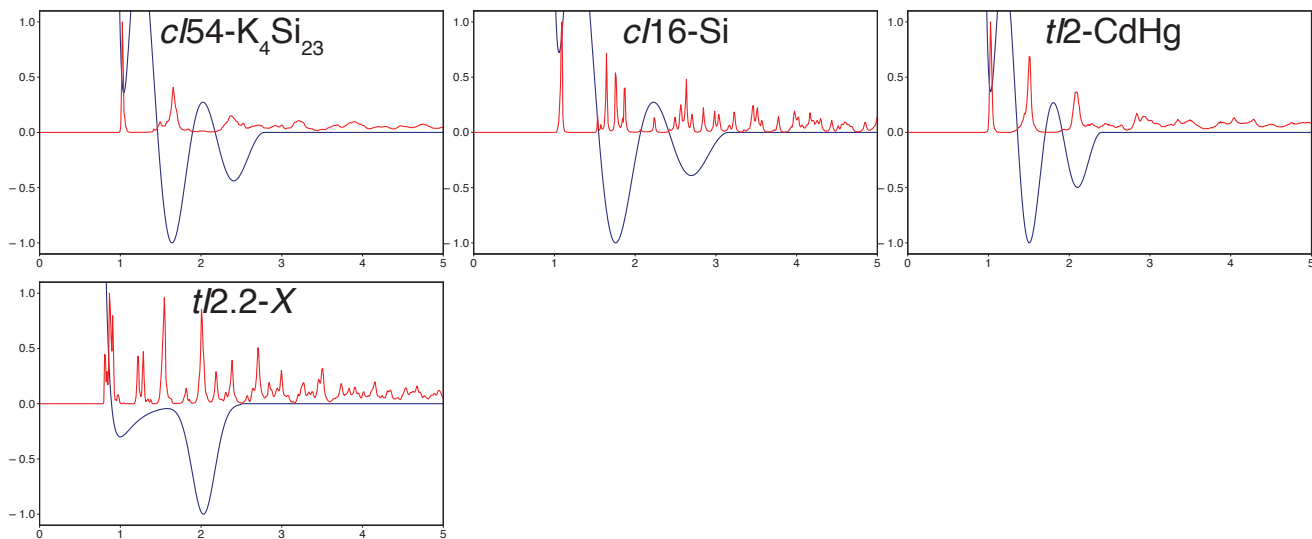
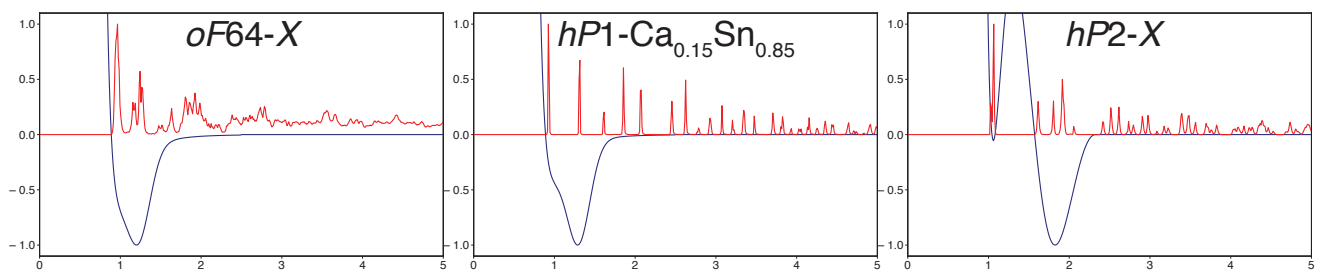**Fig. S12.** Bond-orientational order diagrams (BODs) of the observed structures that have no equivalents on the atomic scale.

Julia Dshemuchadse, Pablo F. Damasceno, Carolyn L. Phillips, Michael Engel, and Sharon C. Glotzer
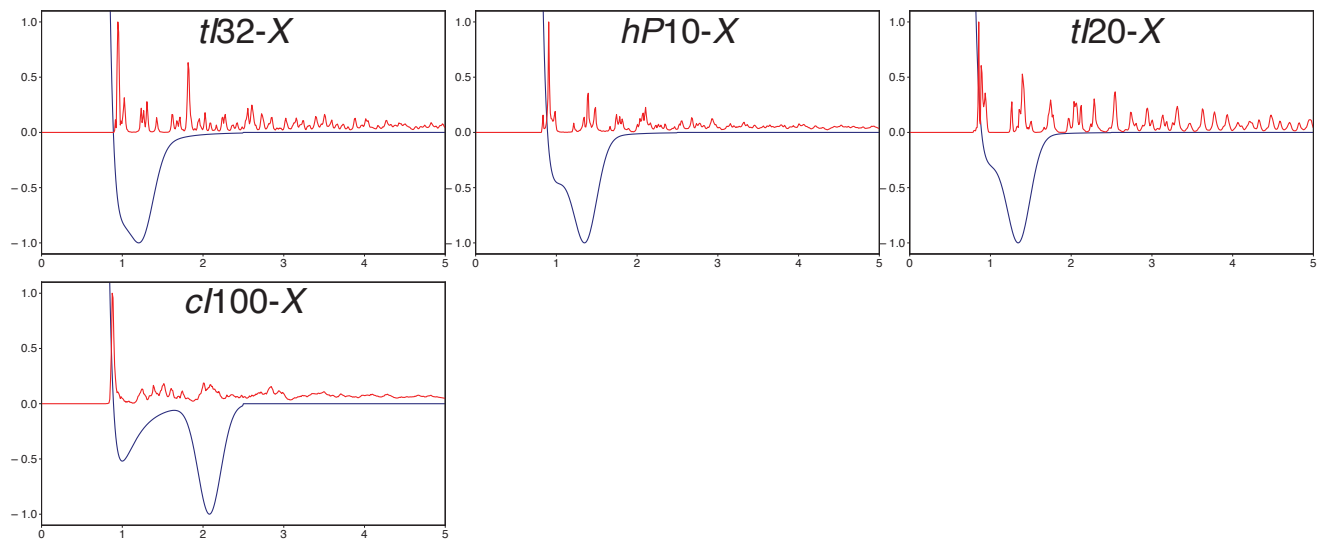
Fig. S13. Potential shapes *(blue)* and radial distribution functions *(red)* of interaction potentials that assemble the $cP54$-K_4Si_{23}, $cI16$-Si, $tI2$-CdHg *(top left-to-right)*, and $tI2.2$-X structures *(bottom)*, all of which have coordination number $CN = 3.4 - 5.0$.
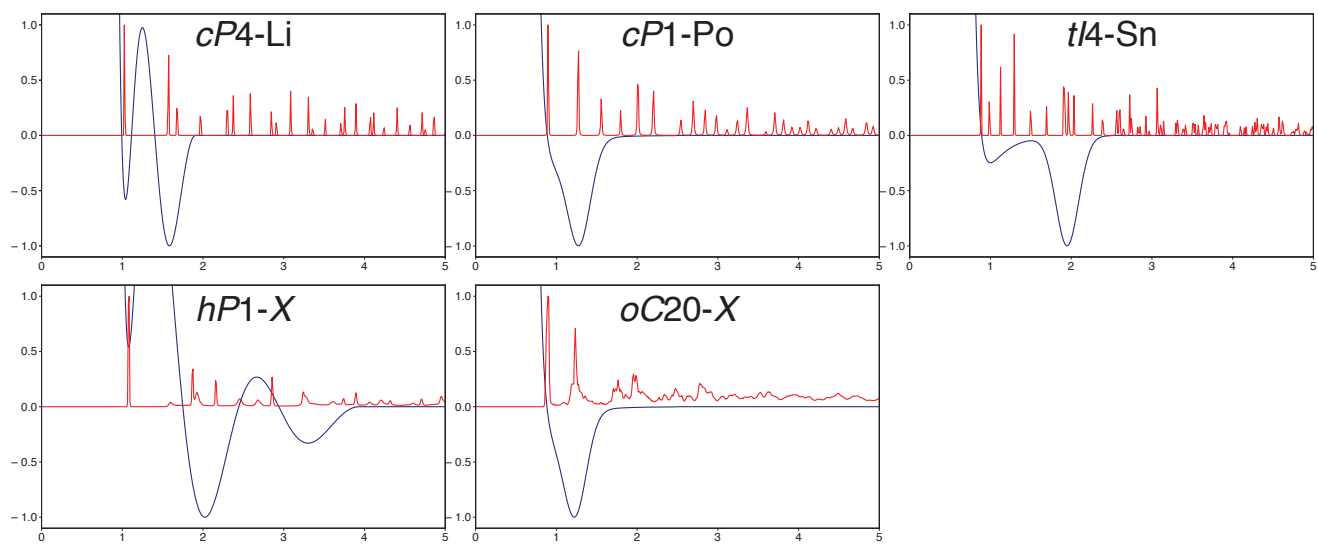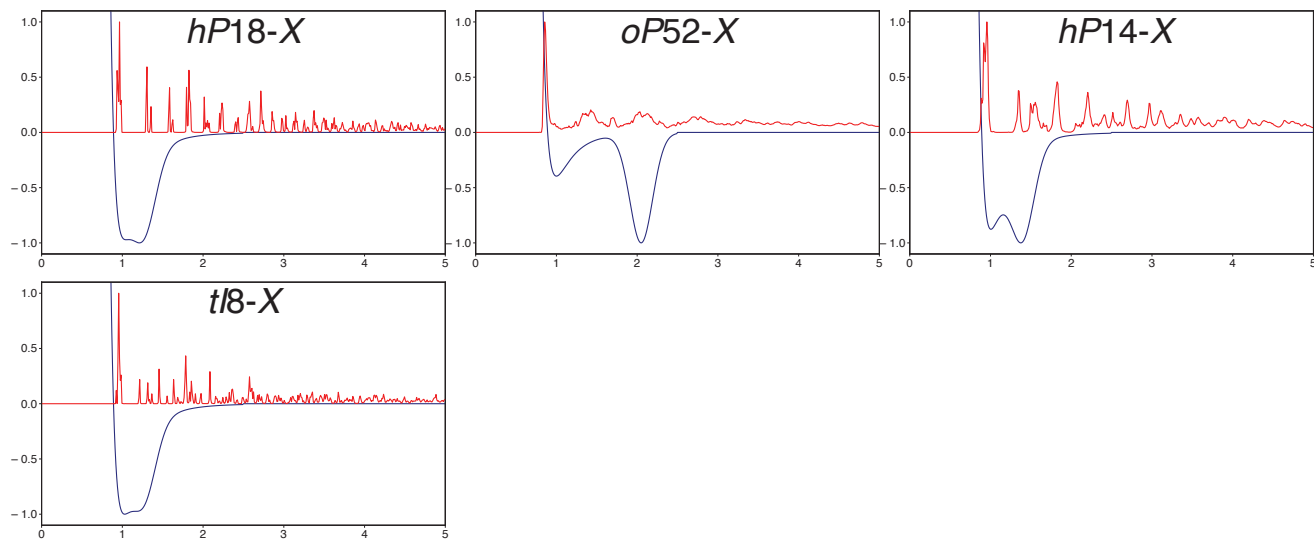
Fig. S14. Potential shapes *(blue)* and radial distribution functions *(red)* of interaction potentials that assemble the $cP4$-Li, $cP1$-Po, $tI4$-Sn *(top row, left-to-right)*, $hP1$-X, and $oC20$-X *(bottom row, left-to-right)* structures, all of which have coordination number $CN = 6$.

Julia Dshemuchadse, Pablo F. Damasceno, Carolyn L. Phillips, Michael Engel, and Sharon C. Glotzer

Fig. S15. Potential shapes *(blue)* and radial distribution functions *(red)* of interaction potentials that assemble the $oF64\text{-}X$, $hP1\text{-}Ca_{0.15}Sn_{0.85}$, and $hP2\text{-}X$ structures *(left-to-right)*, all of which have coordination number $CN = 7.0 - 8$.

Fig. S16. Potential shapes *(blue)* and radial distribution functions *(red)* of interaction potentials that assemble the $tI32\text{-}X$, $hP10\text{-}X$, $tI20\text{-}X$ *(top left-to-right)*, and $cI100\text{-}X$ structures *(bottom)*, all of which have coordination number $CN = 8.8 - 9.3$.

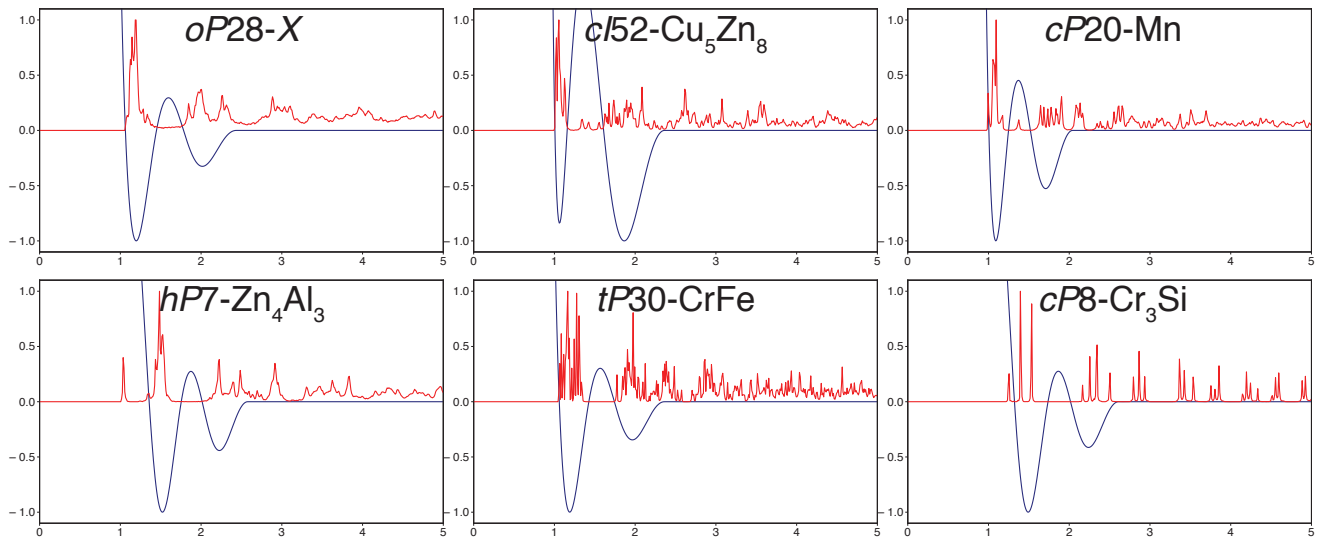**Julia Dshemuchadse, Pablo F. Damasceno, Carolyn L. Phillips, Michael Engel, and Sharon C. Glotzer**

Fig. S17. Potential shapes *(blue)* and radial distribution functions *(red)* of interaction potentials that assemble the $hP18$-X, $oP52$-X, $hP14$-X *(top left-to-right)*, and $tI8$-X structures *(bottom)*, all of which have coordination number $CN = 10.0 - 11.3$.
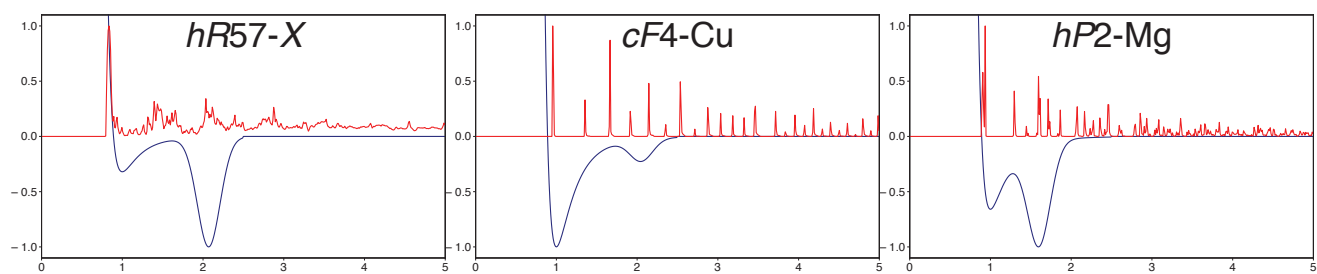
Fig. S18. Potential shapes *(blue)* and radial distribution functions *(red)* of interaction potentials that assemble the $hR57\text{-}X$, $cF4$-Cu, and $hP2$-Mg structures *(left-to-right)*, all of which have coordination number $CN = 12$.

Julia Dshemuchadse, Pablo F. Damasceno, Carolyn L. Phillips, Michael Engel, and Sharon C. Glotzer
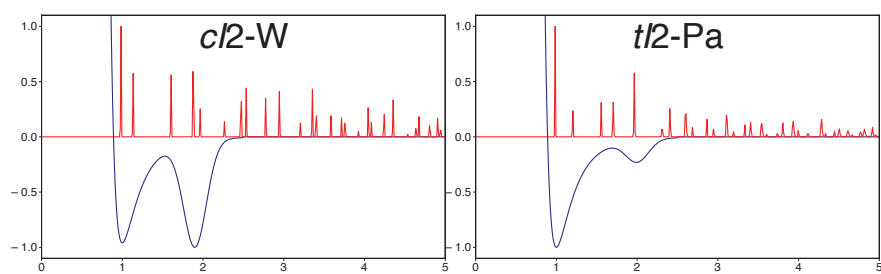
Fig. S19. Potential shapes *(blue)* and radial distribution functions *(red)* of interaction potentials that assemble the $oP28\text{-}X$, $cI52\text{-}Cu_5Zn_8$, $cP20\text{-}Mn$ *(top row, left-to-right)*, $hP7\text{-}Zr_4Al_3$, $tP30\text{-}CrFe$, and $oP8\text{-}Cr_3Si$ *(bottom row, left-to-right)* structures, all of which have coordination numbers $CN = 12.6 - 13.5$.

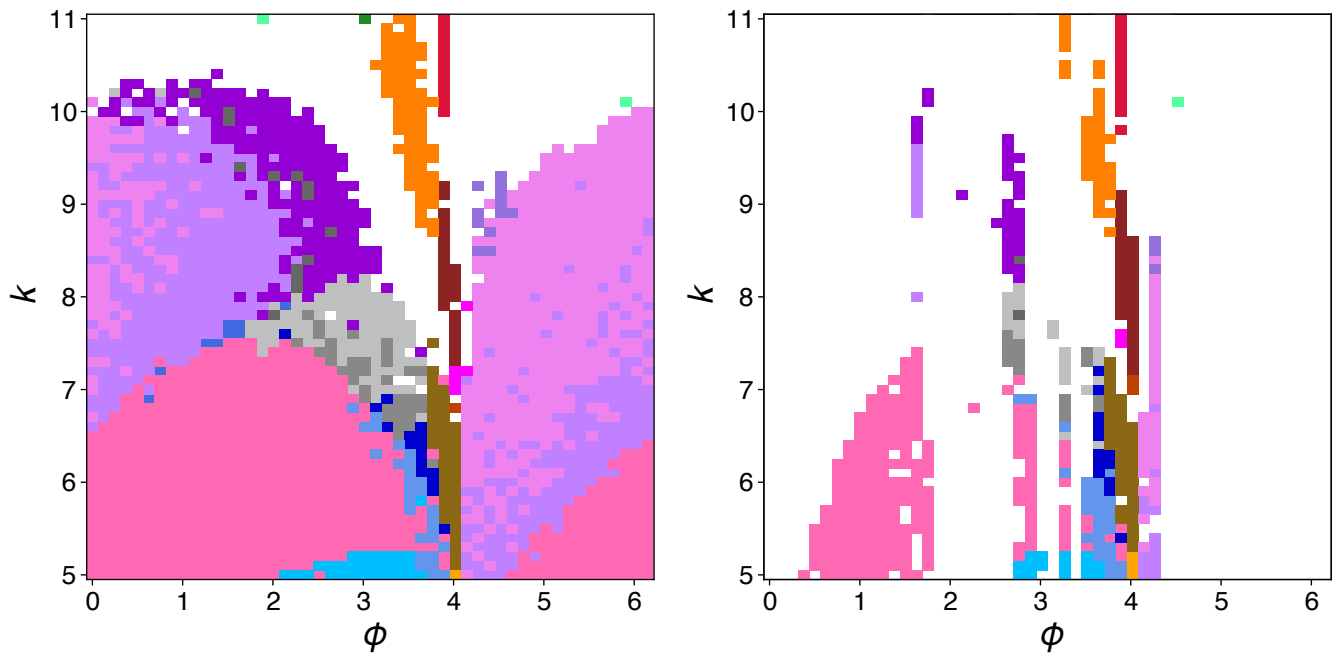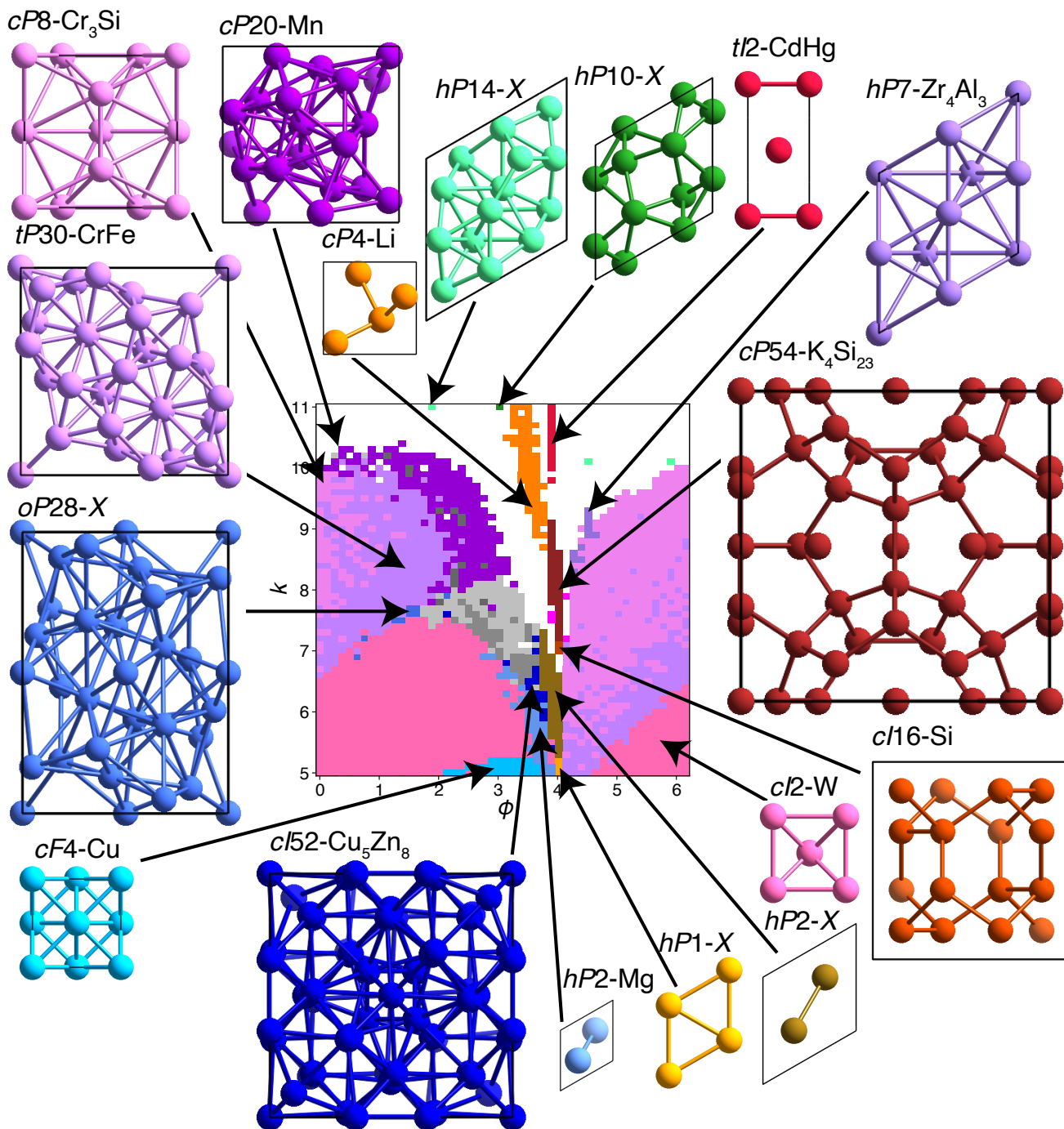**Fig. S20.** Potential shapes *(blue)* and radial distribution functions *(red)* of interaction potentials that assemble the $cI2$-W and $tI2$-Pa structures *(left-to-right)*, all of which have coordination numbers $CN = 14$.

Julia Dshemuchadse, Pablo F. Damasceno, Carolyn L. Phillips, Michael Engel, and Sharon C. Glotzer

Fig. S21. Phase diagrams of the self-assembled crystal structures formed by particles interacting *via* the OPP. The structures assembled in the first and second sweeps of the phase diagram are shown on the left and right.
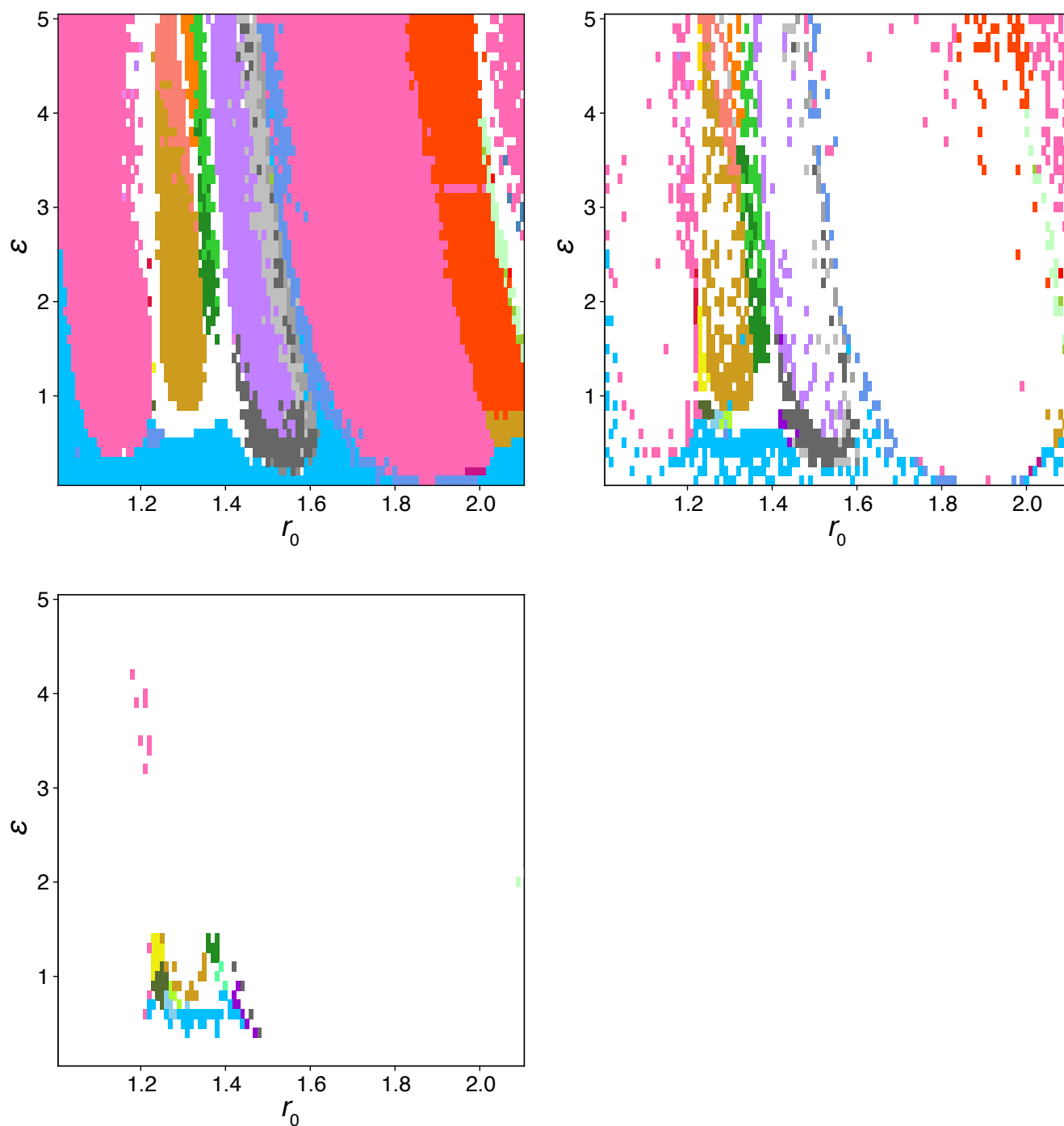
Fig. S22. Phase diagrams of the self-assembled crystal structures formed by particles interacting *via* the LJGP. The structures assembled in the first, second, and third sweeps of the phase diagram are shown in the upper left, upper right, and lower left.

Julia Dshemuchadse, Pablo F. Damasceno, Carolyn L. Phillips, Michael Engel, and Sharon C. Glotzer

Fig. S23. Phase diagrams of the self-assembled crystal structures formed by particles interacting *via* the OPP. The positions of the different crystal phases are indicated and matched with their respective unit cells.

Fig. S24. Phase diagrams of the self-assembled crystal structures formed by particles interacting *via* the LJGP. The positions of the different crystal phases are indicated and matched with their respective unit cells.

Julia Dshemuchadse, Pablo F. Damasceno, Carolyn L. Phillips, Michael Engel, and Sharon C. Glotzer

References

1. HOOMD-blue (https://glotzerlab.engin.umich.edu/hoomd-blue/) (2008–2020).
2. JA Anderson, CD Lorenz, A Travesset, General purpose molecular dynamics simulations fully implemented on graphics processing units. *J. Comput. Phys.* **227**, 5342–5359 (2008).
3. J Glaser, et al., Strong scaling of general-purpose molecular dynamics simulations on GPUs. *Comput. Phys. Commun.* **192**, 97–107 (2015).
4. JA Anderson, J Glaser, SC Glotzer, HOOMD-blue: A Python package for high-performance molecular dynamics and hard particle Monte Carlo simulations. *Comput. Mater. Sci.* **173**, 109363 (2020).
5. M Dutour Sikirić, O Delgado-Friedrichs, M Deza, Space fullerenes: a computer search for new Frank–Kasper structures. *Acta Crystallogr. A* **66**, 602–615 (2010).